



# Secondary Nucleation by Interparticle Energies. I. Thermodynamics

## Journal Article

### Author(s):

Bosetti, Luca ; Ahn, Byeongho ; Mazzotti, Marco

### Publication date:

2022-01-05

### Permanent link:

<https://doi.org/10.3929/ethz-b-000523208>

### Rights / license:

[Creative Commons Attribution-NonCommercial-NoDerivatives 4.0 International](#)

### Originally published in:

Crystal Growth & Design 22(1), <https://doi.org/10.1021/acs.cgd.1c00927>

### Funding acknowledgement:

788607 - Studying Secondary Nucleation for the Intensification of Continuous Crystallization (EC)

## Secondary Nucleation by Interparticle Energies. I. Thermodynamics

Luca Bosetti,\* Byeongho Ahn,\* and Marco Mazzotti\*

Cite This: *Cryst. Growth Des.* 2022, 22, 87–97

Read Online

ACCESS |



Metrics &amp; More



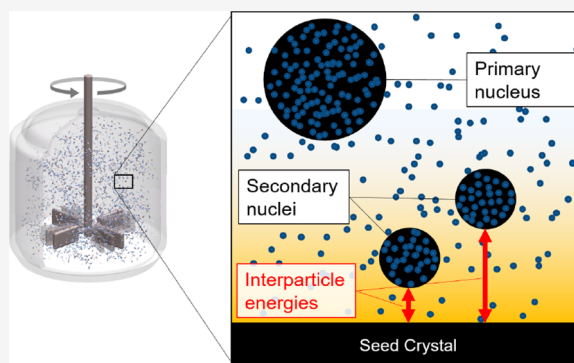
Article Recommendations



Supporting Information

**ABSTRACT:** Secondary nucleation, in the absence of attrition, is known to be dependent on external fields, such as contact forces, shear, or interparticle forces. In this contribution, the thermodynamic effect of the presence of the seed crystal surface on secondary nucleation is derived in the context of the classical nucleation theory. The Gibbs free energy for the formation of a cluster close to a seed crystal is calculated with the addition of interparticle energies, namely, van der Waals attractive forces and Born repulsive forces. This results in the stabilization of a subcritical cluster close to the seed surface that can become a secondary nucleus more easily than under homogeneous nucleation conditions. Far from the seed surface, the developed model is reduced to the homogeneous nucleation described by the classical nucleation theory. The crystallization of paracetamol from an ethanol solution is taken as a case study,

and the stabilization effect, given by the presence of interparticle energies, can be observed at different values of supersaturation. Three key indicators have been defined and calculated to describe the intensity of the stabilization effect, two of which, namely, the distance from the seed surface where the stabilization is active and the enhancement factor for supersaturation, are used in Part II of this series to describe the kinetics of secondary nucleation by interparticle energies.



## 1. INTRODUCTION

Nucleation and growth are two fundamental crystallization processes since they increase the amount of the solid phase at the expense of the liquid phase. In both cases, the driving force for crystallization is a difference in chemical potential,<sup>1</sup>  $\Delta\mu$ , between solute molecules in the liquid phase,  $\mu_{\text{liq}}$ , and in the solid phase,  $\mu_{\text{sol}}$ . When  $\Delta\mu > 0$ , the system experiences supersaturated conditions,<sup>2</sup> and growth, primary and secondary nucleations, can occur following different mechanisms.

Growth mechanisms are usually classified into surface integration-limited and mass transport-limited. Secondary nucleation can be caused by a mechanical mechanism such as attrition, which is not directly dependent on the difference in chemical potential, or by shear and surface phenomena, which require a minimum value of  $\Delta\mu$  to happen, thus resulting in an activated mechanism. This value of  $\Delta\mu$  defines the secondary nucleation threshold. Primary nucleation is defined as heterogeneous, if the nuclei form on an existing surface, or homogeneous if they form in the bulk of the solution. The minimum level of  $\Delta\mu$  that triggers a detectable level of homogeneous nucleation is the primary nucleation threshold.

Secondary nucleation plays a key role in the production of crystals in industrial crystallizers, particularly in the case of continuous crystallization processes, where new crystals generally form in the presence of grown crystals of the same solute. There are various theories to rationalize it.<sup>3–14</sup> The formation of secondary nuclei can be enabled either (i) by mechanical forces originated from the collisions of a seed crystal

with the impeller or with the reactor walls, e.g., in the case of attrition and of initial breeding (see Figure 1a), or else (ii) by the presence of a seed crystal surface that enhances the secondary nucleation process, as it is the case of surface breeding,<sup>8</sup> embryo coagulation,<sup>5</sup> contact nucleation,<sup>12</sup> and shear nucleation<sup>15</sup> (see Figure 1b,c).

Mersmann and co-workers<sup>7,16,17</sup> have developed an extensive theory to model secondary nucleation by attrition, which has been validated by experiments and further expanded in more recent years.<sup>18,19</sup> The main result of these studies is that secondary nucleation by attrition is active at any time because the mechanical forces forming fragments from the seed are only dependent on the stirring conditions. Nevertheless, the secondary nucleation rate depends on  $\Delta\mu$ , since the attrition fragments survive and grow only under supersaturated conditions.<sup>19</sup> It is worth noting that secondary nuclei formed by attrition are of the same nature (polymorphic form or handedness in the case of chiral crystals) as the seed crystal.

The mechanisms based on the effect of the seed crystal surface are less well described and they are usually classified into either contact secondary nucleation or embryo coagulation secondary

Received: August 13, 2021

Revised: October 19, 2021

Published: November 22, 2021



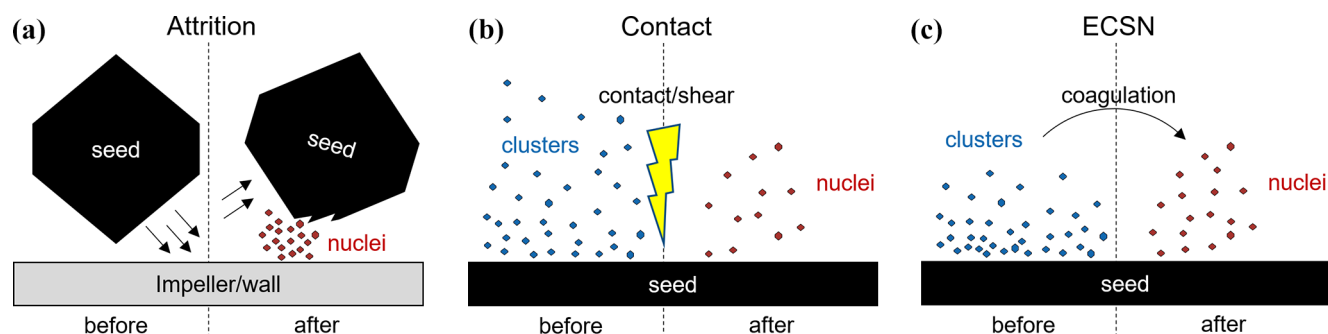


**Figure 1.** Illustration of secondary nucleation mechanisms. (a) Secondary nucleation by attrition after collision with the impeller/wall. (b) Surface-induced secondary nucleation due to contact/shear. (c) Embryo coagulation secondary nucleation.<sup>5</sup>

nucleation (ECSN). In contact secondary nucleation, on the one hand, clusters that are already formed in solution<sup>20,21</sup> nucleate when close to a seed crystal because of the contact with an external body (e.g., impelling rod<sup>9–11,22</sup>) because of fluid shear<sup>15,23–25</sup> or because of an “autocatalytic” effect of the crystal surface.<sup>13</sup> On the other hand, according to the ECSN theory,<sup>5</sup> the van der Waals forces between clusters and seed crystal enhance the concentration of clusters close to the seed, and secondary nuclei result from the rapid coagulation of those clusters. Nuclei produced by surface-induced secondary nucleation shall not necessarily have the same polymorphic form or handedness as the seed crystal.

In summary, the seed crystal surface might work as a catalyst for the formation of clusters. This mechanism has been experimentally observed,<sup>10,26</sup> and it has been used to explain the non-stereo-selective nucleation of enantiomers.<sup>8,27</sup>

In this context, this contribution presents a novel thermodynamic framework to describe secondary nucleation by interparticle energy, SNIPE in short, as a homogeneous primary nucleation mechanism, enhanced by the presence of seed crystals. As a matter of fact, in solution, some clusters get energetically stabilized by the presence of the seed surface. The Gibbs free energy for the formation of a cluster is calculated according to classical nucleation theory (CNT),<sup>1</sup> with the addition of a contribution due to interparticle interactions acting between the seed surface, and the molecules and clusters in solution and suspension, respectively. In recent years, an alternative nucleation theory, i.e., the two-step nucleation theory, has been introduced, based on the observation of the presence of dense-liquid structures during the process of formation of nuclei. This theory has originally been developed for large molecules, i.e., proteins,<sup>28,29</sup> but dense-liquid structures have also been observed in the case of small organic and inorganic molecules.<sup>30,31</sup> In principle, the framework of SNIPE could be applied to the two-step nucleation theory as well: the interparticle energies between the dense-liquid structure and the seed crystal would describe the effect of SNIPE, provided the full energetic characterization of the intermediate state, i.e., an analytical expression of the energy of formation of nuclei from the two-step nucleation process, was available. Nevertheless, in this work, we perform the analysis starting from the description given by the CNT, which is a well-accepted theory, whose functional form is able to describe experimental results, and which has been used to characterize the primary nucleation of a broad range of materials. Summarizing, due to interparticle interactions, the primary nucleation process is facilitated and accelerated. Similarly to ECSN, SNIPE involves interactions among clusters and seed surface, but contrary to ECSN, SNIPE

does not attribute the formation of stable secondary nuclei to coagulation. SNIPE’s approach is firmly rooted in the simple concepts of the classical nucleation theory.

This paper is structured as follows: in Section 2, we present the thermodynamic formulation of the Gibbs free energy for the formation of a cluster in the proximity of the seed crystal surface. This requires a detailed understanding of the solute concentration around growing crystals and of the interparticle forces. Then, in Section 3, a case study of paracetamol crystallization in an ethanol solution at a constant supersaturation is examined and discussed; in particular, three key quantities are defined to quantify the effect of interparticle interaction on the nucleation process. Finally, in Section 4, a sensitivity analysis on two uncertain parameters is carried out and the thermodynamic description of ECSN is compared to that of SNIPE.

## 2. THERMODYNAMICS

In the scope of the classical nucleation theory, CNT in short, external fields, such as gravity, attractive, and repulsive interparticle forces, are not considered. Inspired by the research on colloidal systems,<sup>32–37</sup> we include the effect of interparticle forces into the classical framework of crystal nucleation. In the following, the thermodynamics for the formation of a cluster near a seed crystal surface is described: to this aim, one needs to determine the solute concentration near the surface of a growing seed crystal and to define the possible interparticle interactions in the system. Finally, we include this newly derived Gibbs free energy into the conceptual framework of CNT, including by using the concept of critical nucleus size.

**2.1. Gibbs Free Energy for the Cluster Formation Near a Crystal Surface.** Let us now consider the Gibbs free energy required for the formation of a single cluster consisting of  $n$  molecules in the proximity of a seed surface. In this case, we assume that in the initial state, i.e., State 1 in Figure 2,  $M$  solute molecules (we are considering for the sake of simplicity but without loss of generality molecules that do not dissociate in solution) dissolved in a solvent in the proximity of a seed crystal of the same substance. The Gibbs free energy for State 1 can be written as

$$G_1 = M\mu_1 + G_{se} + \sum_{i=1}^M E_{IP}^m(x_i) \quad (1)$$

where  $\mu_1$  is the chemical potential of a solute molecule in the solution (in units of J per molecule),  $G_{se}$  is the free energy of the seed, and  $E_{IP}^m$  is the interparticle energy between a dissolved molecule and the seed surface, which depends on the distance  $x_i$  between the two.

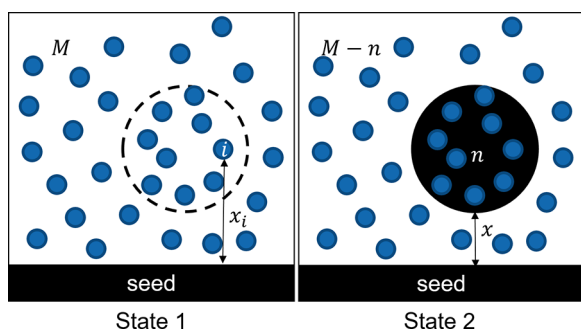


**Figure 2.** Formation of a cluster of  $n$  molecules. State 1 consists of  $M$  solute molecules in solution and the surface of a seed crystal (in black). Each molecule  $i$  is at distance  $x_i$  from the seed surface. State 2 represents the situation after the formation of  $n$ -molecule clusters at a distance of  $x$  from the crystal surface. The number of dissolved solute molecules decreases to  $M - n$ . Solvent molecules are considered to be inert as in CNT and not visualized for clarity.

State 2 in Figure 2 shows the final state after the formation of the cluster; its Gibbs free energy can be calculated as

$$G_2 = (M - n)\mu_1 + n\mu_c + G_{\text{se}} + b\gamma n^{2/3} + \sum_{i=1}^{M-n} E_{\text{IP}}^m(x_i) + E_{\text{IP}}^c(n, x) \quad (2)$$

where  $n$  is the number of molecules in the cluster, with chemical potential equal to  $\mu_c$ ,  $b$  is the surface area of a molecule, i.e., a sphere in this case hence  $b = \pi d_1^2 = (36\pi)^{1/3} V_1^{2/3}$ ,  $\gamma$  is the specific surface energy, and  $E_{\text{IP}}^c(n, x)$  is the interparticle energy between the  $n$ -sized cluster and the seed surface, depending on the distance  $x$  between the two.

To describe the process, the following assumptions are introduced:

- (1) the surface of the seed crystal is considered as a flat surface, infinitely larger than the cluster forming in its proximity;
- (2) the size of the cluster is characterized by the number of constituting molecules, and the cluster shape is assumed to be spherical;
- (3) the positions of the  $n$  molecules in State 1 are identical to those of the  $n$  molecules forming the  $n$ -sized cluster in State 2. In the Supporting Information, other geometric configurations of the  $n$  molecules in solution (i.e. before cluster formation) are considered and their effect on the interparticle energy and on the secondary nucleation is discussed; such analysis shows that the configuration described above represents the most consistent approach.

It is worth noting that the last term on the right-hand side of eq 2 depends only on the cluster size,  $n$ , and on its distance from the seed surface,  $x$ , because the position of the individual molecules in the cluster is uniquely specified when assigning  $n$  and  $x$  (see Figure 2). This is true also for the last term on the right-hand side of eq 1 because of assumption 3 (see eq 6).

The Gibbs free energy change upon the formation of an  $n$ -sized cluster in the proximity of a seed crystal is therefore

$$\Delta G = G_2 - G_1 = \underbrace{-n\Delta\mu}_{\Delta G_V(\Delta\mu, n)} + \underbrace{b\gamma n^{2/3}}_{\Delta G_A(n)} + \underbrace{E_{\text{IP}}^c(n, x) - \sum_{i=1}^n E_{\text{IP}}^m(x_i)}_{\Delta G_{\text{IP}}(n, x)} = \quad (3)$$

$$= \Delta G_{\text{hon}}(\Delta\mu, n) + \Delta G_{\text{IP}}(n, x) \quad (4)$$

where the change in chemical potential per molecule is  $\Delta\mu = \mu_1 - \mu_c$ . In eq 3, we highlight the three components of  $\Delta G$ , all dependent on the cluster size,  $n$ .  $\Delta G_V$  is the only term dependent on  $\Delta\mu$ , and it is always negative.  $\Delta G_A$  is the cluster surface energy, and it is always positive.  $\Delta G_{\text{IP}}$  is the interparticle potential, which can, in principle, be positive or negative, depending on the distance from the seed surface,  $x$ . The sum of  $\Delta G_V$  and  $\Delta G_A$  is the Gibbs free energy of formation of an  $n$ -sized cluster for homogeneous nucleation in the scope of CNT,  $\Delta G_{\text{hon}}(\Delta\mu, n)$ .<sup>1,2</sup> The interparticle term is novel with respect to the CNT; it can be viewed as the effect of an external field, namely, that created by the seed crystal itself.

To calculate the total Gibbs free energy, the following quantities need to be determined:  $\Delta\mu$  close to the seed surface and the interparticle energies.

**2.1.1. Concentration Profile at the Interface of a Growing Crystal.** The driving force of crystallization is often related to the supersaturation ratio,  $S$ , defined as<sup>2</sup>

$$\ln S = \ln \frac{c}{c^*} \approx \frac{\Delta\mu}{k_B T} \quad (5)$$

where  $c$  is the solute concentration in the liquid phase,  $c^*$  is the bulk solubility,  $k_B$  is the Boltzmann constant, and  $T$  is the absolute temperature of the solution. The approximation in eq 4 holds for conditions where the ratio of the solute's activity coefficients at  $c$  and  $c^*$  is close to 1.<sup>1,2,38</sup>

In the supersaturation regime, where growth and secondary nucleation are active, molecules in a supersaturated solution attach to an existing crystalline surface. This is a problem regarding mass transfer and kinetics of attachment and detachment at the crystal surface; thus, a description of the concentration at the liquid–solid interface is needed.<sup>2</sup> The supersaturation at the interface is what we believe to be the driving force for secondary nucleation in the proximity of a seed crystal,<sup>39,40</sup> and because of considerations about the growth regimes, reported in the Supporting Information, it is reasonable to assume that the interfacial supersaturation is equal to the bulk supersaturation,  $S_i \approx S$ . In the Supporting Information, we provide additional material to support this conclusion, i.e., a description of the crystal growth theories,<sup>7,41–44</sup> and an overview of experimental works<sup>45,46</sup> that measure the concentration close to a growing crystal.

**2.1.2. Interparticle Energies.** The interaction potential between a spherical cluster and an infinitely large surface in the geometry described in Figure 2 can be calculated using the method developed by Hamaker,<sup>47</sup> where pairwise additivity of the intermolecular forces is assumed. The full derivation of the equations hereafter can be found in the Supporting Information; here, we only present the final form.

Considering both van der Waals attractive forces and Born repulsive forces (soft repulsion),<sup>33,34,48</sup> the interparticle potential for an  $n$ -sized cluster can be written as

$$E_{\text{IP}}^c(n, x) = \underbrace{-\frac{A_c}{6} \left[ \frac{2R_n(x + R_n)}{x(x + 2R_n)} - \ln \left( 1 + \frac{2R_n}{x} \right) \right]}_{E_{\text{vW}}^c < 0} + \underbrace{\frac{A_c \sigma_0^6}{7560} \left[ \frac{8R_n + x}{(2R_n + x)^7} + \frac{6R_n - x}{x^7} \right]}_{E_{\text{B}}^c > 0} \quad (6)$$

where  $x$  is the distance between the surface of the cluster and that of the seed crystal;  $R_n = n^{1/3} R_1$  is the radius of the  $n$ -sized cluster, with  $R_1$  being the molecular radius;  $A_c$  is the Hamaker constant for the cluster interacting with the seed crystal; and  $\sigma_0$  is the collision diameter of the Born repulsive forces. The sum of the interaction energies of the  $n$  molecules in solution before they form the cluster can be calculated with the same

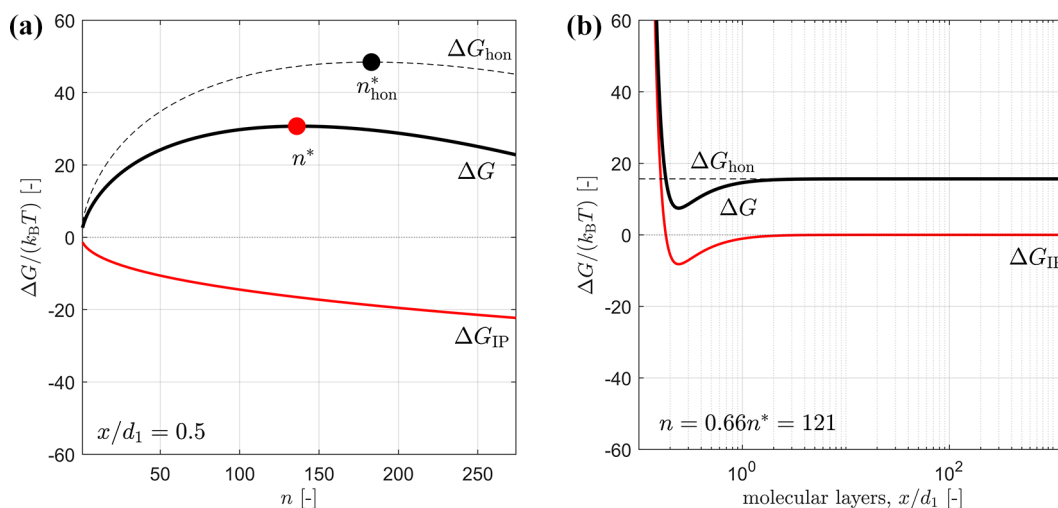


**Figure 3.** Decomposition of the total Gibbs free energy (solid black), in its interparticle (solid red) and homogeneous nucleation (dashed black) components as in eq 4. (Left) Critical nucleus sizes are indicated as the size corresponding to the maximum of the total Gibbs free energy, both for the stabilized case (red circle) and for the homogeneous case (black circle). (Right) Total energy, when getting closer to the seed surface, presents a well, which is the cause of the stabilization compared to the homogeneous nucleation conditions.

geometrical considerations as in the Hamaker method, and it results in

$$\sum_{i=1}^n E_{\text{IP}}^{\text{m}}(x_i) = \frac{A_{\text{m}}}{A_{\text{c}}} E_{\text{IP}}^{\text{c}}(n, x) \quad (7)$$

where  $A_{\text{m}}$  is the Hamaker constant of a dissolved molecule interacting with the seed crystal and the energy of the molecule is calculated as the energy of a cluster of size 1 at a distance  $x$  from the surface; thus,  $E_{\text{IP}}^{\text{m}}(x) = A_{\text{m}}/A_{\text{c}} E_{\text{IP}}^{\text{c}}(1, x)$ .

For ionic systems such as NaCl or KCl, where solute molecules are dissociated into ions, the contribution of electrostatic energy must be considered in addition to the van der Waals and Born contributions. In this case, the thermodynamic analysis can be based on the considerations above, but a different interparticle potential has to be considered. In particular, the electrostatic contribution would result in the formation of a Stern double layer,<sup>48</sup> or in more complex ionic concentration profiles along the distance (from the seed surface) coordinate,<sup>49</sup> which would substantially modify the energy landscape close to the seed surface itself. Studies of molecular dynamics have shown the formation of clusters of NaCl in an aqueous solution close to a seed crystal.<sup>49</sup> In other works, the mechanisms of nucleation of ionic crystals, independently of the presence of seeds, have been investigated,<sup>50,51</sup> starting from an interparticle potential comprising van der Waals attraction, Born repulsion, and electrostatic energies.<sup>52</sup> In case different solvents are considered, the choice of interparticle energies needs to be revised according to their physical and chemical properties (e.g., polarity, viscosity, and density), as well as to their possible interaction with the solute, thus resulting in an interparticle potential including other contributions, e.g., electrostatic, drag, friction, and shear forces.<sup>48</sup>

In the **Supporting Information**, we provide details about the mathematical derivation, in fact, an integration, to obtain the cluster surface and the molecule surface potentials, as well as an analysis about different interparticle forces, e.g., the DLVO theory, and further considerations about  $A_{\text{c}}$  and  $A_{\text{m}}$ .

**2.2. Total Gibbs Free Energy.** Substituting eqs 4, 5, and 6 into eq 3, one can express the Gibbs free energy change upon the formation of an  $n$ -sized cluster as

$$\Delta G(S, n, x) = -nk_{\text{B}}T \ln S + b\gamma n^{2/3} + \left(1 - \frac{A_{\text{m}}}{A_{\text{c}}}\right) E_{\text{IP}}^{\text{c}}(n, x) \quad (8)$$

which can be plotted either as a function of the number of molecules in the cluster,  $n$  (see Figure 3a), or as a function of the distance from the seed surface,  $x$  (see Figure 3b).

The total Gibbs free energy as a function of the distance to the seed crystal (solid black line in Figure 3b) exhibits a minimum at around 0.3 molecular layers, which yields a stabilization effect to the cluster compared to that experienced by the same cluster in the bulk of the solution, i.e., under conditions where only homogeneous nucleation may occur. The stabilization effect is given by the fact that, at small distances from the seed surface, the energetic barrier to overcome to form a cluster,  $\Delta G$ , is lower than the energetic barrier for homogeneous nucleation,  $\Delta G_{\text{hon}}$  (see the dashed black line in Figure 3b).

The dependence of  $\Delta G$  on  $n$ , as illustrated in Figure 3a, is qualitatively similar to that obtained through CNT, i.e., when the term  $\Delta G_{\text{IP}}$  is not present. As in the CNT,<sup>39</sup> the critical nucleus size,  $n^*$ , is the size at which the Gibbs free energy reaches its maximum, and it can be calculated as

$$n^*(S, x): \left. \frac{\partial \Delta G(S, n, x)}{\partial n} \right|_{n^*(S, x)} = 0 \quad (9)$$

for every distance  $x$  from the seed crystal. The stabilization effect produced by the seed surface is also evident because of the smaller critical nucleus size (red circle in Figure 3a) compared to the critical nucleus size for homogeneous primary nucleation based on CNT (black circle in Figure 3a), and by the correspondingly lower  $\Delta G$  value at the maximum of the curve, i.e., by the lower energy barrier for the formation of a stable nucleus.

Because of the effects quantified by eq 7 and illustrated in Figure 3, the formation of new stable nuclei is favored in the proximity of a seed crystal with respect to the bulk of the

solution. The “depression” of the critical  $\Delta G$  barrier shown in Figure 3 is enough to justify a higher rate of nuclei formation in the presence of seeds, than in the bulk of the solution. In crystallization processes, such an effect will be related, possibly in a proportional manner, to the overall surface area provided by the seeds. The combination of these two features of the mechanism described here motivates us to call it indeed secondary nucleation.

### 3. RESULTS

In this section, we present the results of our analysis, in terms of the energy landscape resulting from the implementation of the SNIPE theory and of the effect of supersaturation. We also define useful indicators of the stabilization effect. All calculations are based on parameters that characterize the behavior of paracetamol in an ethanol solution (see Table 1).

**Table 1. Physical and Chemical Properties of the Paracetamol–Ethanol System at 20 °C<sup>a</sup>**

symbol	paracetamol	description
$\rho_c$	1263	crystal density [kg/m <sup>3</sup> ]
$\rho_l$	789	solution density [kg/m <sup>3</sup> ]
$M_W$	$151.16 \times 10^{-3}$	molar mass [kg/mol]
$c^*$	0.18	solubility concentration at 20 °C [kg/kg]
$\gamma$	$11.1 \times 10^{-3}$	specific surface energy [J/m <sup>2</sup> ]
$k_v$	$\pi/6$	volume shape factor
$V_1$	$1.99 \times 10^{-28}$	molecular volume [m <sup>3</sup> ]
$A_c$	$1 \times 10^{-19}$	cluster Hamaker constant [J]
$A_m/A_c$	0.05	ratio of molecule-cluster Hamaker constants
$\sigma_0$	$0.3 \times 10^{-9}$	collision diameter [m]

<sup>a</sup>Solubility data from Worlitschek and Mazzotti.<sup>53</sup> The value of the specific surface energy is within the range between an experimentally fitted value ( $4.3 \times 10^{-3}$  J/m<sup>2</sup> at 40–46 °C in ref 54) and a theoretically predicted value ( $13.4 \times 10^{-3}$  J/m<sup>2</sup> at 20 °C by eq 12 in ref 55).

**3.1. Energy Landscape of SNIPE.** At a given supersaturation, i.e., for a given value of  $\Delta\mu$ , there are only three free parameters to fully determine eqs 5 and 6, namely, the Hamaker constant of clusters,  $A_c$ , the Hamaker constant of molecules,  $A_m$ , and the collision diameter,  $\sigma_0$ . The ratio between the molecule and the cluster Hamaker constants is set to 0.05 since we assume that molecules dissolved in solution have similar, if not the same, refractive index and dielectric constant as the solution, thus resulting in  $A_m \ll A_c$  and in a weak interaction of molecules with the seed crystal. A more detailed explanation is provided in the Supporting Information. The value of the Hamaker constant and of the collision diameter (reported in Table 1) have been taken from the literature,<sup>33,34,48</sup> and a sensitivity analysis, where both of them are varied, is presented in Section 4.1.

In Figure 4, the Gibbs free energy for the formation of a cluster, as given by eq 3, is shown as a function of the cluster size,  $n$ , and of the distance from the surface rescaled by the molecular diameter,  $x/d_1$  (we will call this the number of molecular layers). This energetic landscape is valid for a fixed value of supersaturation, namely,  $S = 1.7$  in this case, while qualitatively similar but quantitatively different results are obtained at different levels of supersaturation (see Figure 5). Note that the color code of  $\Delta G$  is identical in Figures 4 and 5; warm colors in Figures 4 and 5, e.g., light green and yellow, correspond to large values of  $\Delta G$ , while cold colors, e.g., dark green and blue, correspond to small ones. The critical nucleus size is defined by

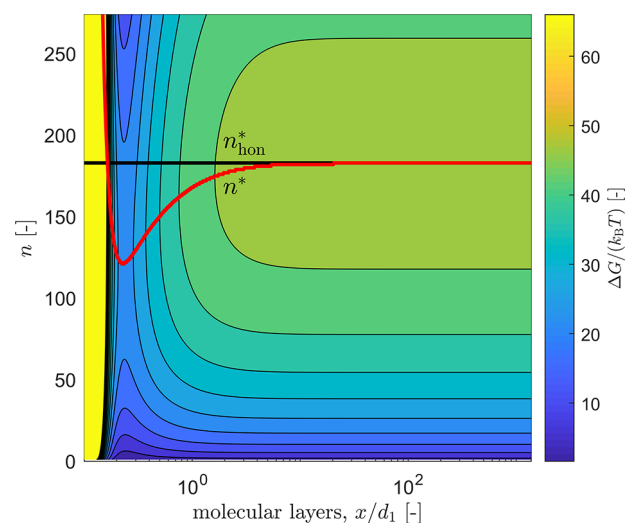


**Figure 4.**  $\Delta G$  as a function of the cluster size,  $n$ , and the distance from the seed surface,  $x/d_1$ . The critical nucleus size, calculated according to eq 8, is shown with a solid red curve, and the CNT critical nucleus size, which is independent of distance, is shown with a solid black line.

eq 8, and it is plotted in Figure 4 as a function of the distance from the seed surface as a red line. Note that the CNT critical nucleus size,  $n_{\text{hon}}^*$ , plotted as a black line, is obviously independent of this distance.

In Figures 4 and 5, one can readily observe that  $\Delta G$  attains very high values close to the surface, thus resulting in an extremely large, almost infinitely large, critical nucleus size. Then, the critical nucleus size reaches a minimum value, at about 0.3 molecular layers, before approaching asymptotically the same plateau value calculated with CNT for homogeneous nucleation.

With reference to Figure 4, by changing the distance from 0.3 to 10 molecular layers, the critical nucleus size changes from about 120 to about 180 molecules, and the dimensionless energy barrier to overcome, i.e.,  $\Delta G/(k_B T)$ , from about 25 to about 45: this demonstrates the stabilization effect on clusters due to the interparticle energies at a small distance from the seed surface. In this work, we do not discuss if these clusters survive and how they are exchanged back and forth with the bulk, but we just present the thermodynamic aspects related to the possibility of the formation of supercritical nuclei at certain distances from the seed surface. The kinetics aspects of this model are reported in Part II of this series.<sup>56</sup>

In Figure 5, we show the same results for  $\Delta G$ , as in Figure 4, at two other supersaturation levels, namely,  $S = 1.5$  and 1.9. There, the energy landscapes have similar topology and structure but different quantitative values. It is worth noting that when  $S$  increases from 1.5 to 1.7 and to 1.9, the smallest critical size decreases from about 300 molecules to about 120 and to about 70, whereas the minimum in the dimensionless energy barrier drops from about 45 to about 25 and to about 15. This result is straightforward, meaning that, at higher supersaturation, nucleation occurs more easily and the critical nucleus is smaller.

**3.2. Stabilization Indicators.** To quantify the enhancement effect of the interparticle potential on secondary nucleation, three dimensionless quantities are defined: the supersaturation enhancement factor,  $E_{\text{st}}$  (in Section 3.2.1), the stabilization distance,  $l_{\text{st}}$  (in Section 3.2.2), and the maximum relative decrease in critical nucleus size,  $\lambda^*$  (in Section 3.2.3).

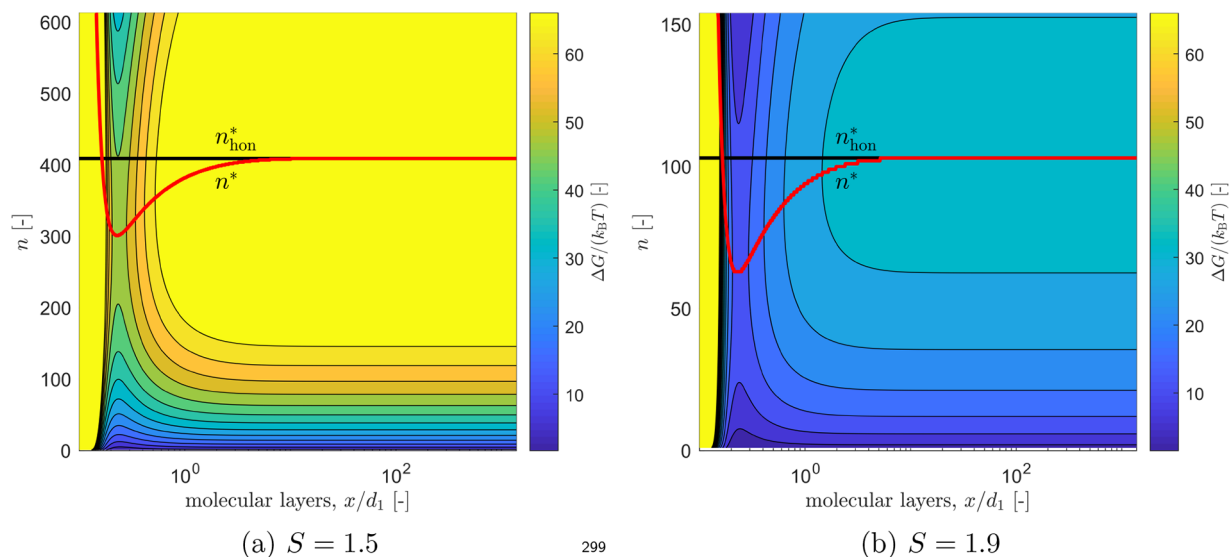


**Figure 5.**  $\Delta G$  as a function of the cluster size,  $n$ , and the distance from the seed surface,  $x/d_1$ , at two values of supersaturation, namely,  $S = 1.5$  (left) and  $S = 1.9$  (right). The critical nucleus size is shown with a solid red curve and calculated with eq 8; the homogeneous critical size is shown with a solid black line.

These indicators are needed to compare different conditions and different systems, e.g., when varying supersaturation.

**3.2.1. Supersaturation Enhancement Factor.** The supersaturation enhancement factor is defined as

$$E_{st}(n, x) := \exp\left(-\frac{1}{n} \frac{\Delta G_{IP}(n, x)}{k_B T}\right) \quad (10)$$

where  $\Delta G_{IP}$  is defined in eqs 3 and 4 and shown in Figure 6, for the case  $S = 1.7$ . By varying  $n$  over all of the possible cluster sizes, we obtain  $\tilde{x}_n$ , which is the locus corresponding to the minima of  $\Delta G_{IP}(n, x)$  with respect to  $x$ , and it is shown with a dashed red line in Figure 6. In this plot,  $n^*$  and  $n_{hon}^*$  are again the SNIPE and the CNT critical nucleus size, respectively. The minimum

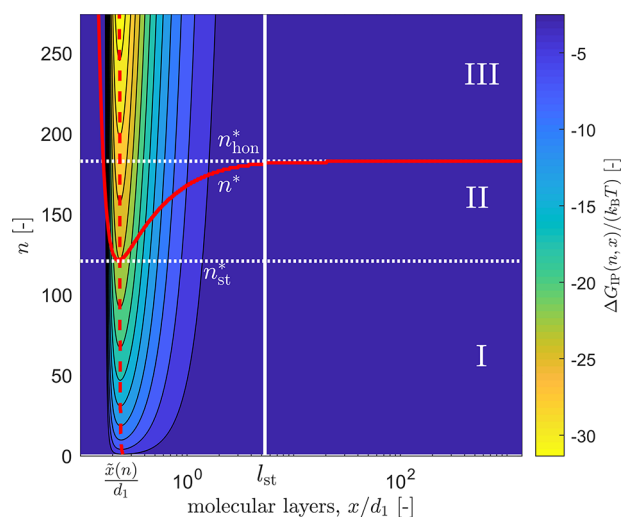


**Figure 6.**  $\Delta G_{IP}(n, x)$  as a function of  $n$  and  $x$ , the locus corresponding to the minima of  $\Delta G_{IP}(n, x)$  is shown with a dashed red line,  $\tilde{x}_n$ , and the nondimensional stabilization distance,  $l_{st}$ , with a dashed white line. The critical nucleus size is shown with a solid red curve, and the homogeneous critical size is shown with a solid white line.  $n_{st}^*$  corresponds to the minimum critical nucleus size because of the stabilization effect.

critical size of SNIPE is defined as  $n_{st}^* = \min_x(n^*(x))$ . Using these definitions, the stabilization energy landscape of Figure 6 can be subdivided into three distinct regions: (i) region I, if  $1 < n < n_{st}^*$ , where a cluster gets stabilized but its size is smaller than the critical size; (ii) region II, if  $n_{st}^* < n < n_{hon}^*$ , where a cluster can undergo SNIPE, but not homogeneous nucleation; and region III, if  $n > n_{hon}^*$ , where the size of the cluster is larger than the CNT critical nucleus size for homogeneous nucleation, and both this and SNIPE can occur.

It is worth noting that SNIPE is favored over homogeneous nucleation because the stabilization effect decreases the energy barrier for the formation of a cluster, whose effect is twofold: on the one hand, the critical size gets smaller, thus allowing a small cluster to become a nucleus (e.g., a cluster in region II), but on the other hand, the interparticle energies also increase the concentration of clusters in the stabilized region, thus enhancing indirectly the rate of nucleation, as explained in Part II of this series.<sup>56</sup>

By solving eq 9 for  $\Delta G_{IP}$  and by substituting it into eqs 4 and 7, one can rewrite  $\Delta G$  as

$$\Delta G(S, n, x) = -nk_B T \ln(SE_{st}(n, x)) + byn^{2/3} \quad (11)$$

where the effect of interparticle energies is represented by a single factor  $E_{st}$  by which the supersaturation is multiplied. Note that, setting  $E_{st} = 1$ , i.e., no effect of interparticle interactions, reduces eq 10 to the  $\Delta G$  expression for homogeneous nucleation according to CNT.

**3.2.2. Stabilization Distance.** As discussed above and illustrated in Figures 4–6, the stabilization effect is active only up to a certain distance from the seed surface,  $x_{st}$ , beyond which it vanishes and the critical nucleus size is equal to that of homogeneous nucleation. This stabilization distance can be quantified by the following dimensionless distance,  $l_{st} = x_{st}/d_1$ . Let us first define the relative decrease in critical nucleus size as

$$\nu(S, x) = \frac{n_{hon}^*(S) - n^*(S, x)}{n_{hon}^*(S)} \quad (12)$$

which is a relative measure of the distance between the SNIPE critical nucleus size,  $n^*(S, x)$ , and the CNT critical nucleus size,  $n_{\text{hon}}^*(S)$ . The stabilization distance is defined as the biggest  $x$  where  $\nu(S, x)$  is larger than an arbitrary value  $\epsilon$ , i.e.,

$$x_{\text{st}}(S) = \max_x \nu(S, x) \quad (13)$$

$$\text{s.t. } \nu(S, x) \geq \epsilon \quad (14)$$

In the examples reported in this paper,  $\epsilon$  is set to 0.01. In Figure 6, the nondimensional stabilization distance  $l_{\text{st}}$  is shown by a vertical solid white line, which divides the plane into two regions: on the left-hand side, the cluster formation is facilitated by the stabilization effect (i.e., by negative values of  $\Delta G_{\text{IP}}$  in an interval of distances from the seed surface), whereas on the right-hand side, the stabilization effect is absent (i.e.,  $\Delta G_{\text{IP}}$  is negligible). Note that the sign of  $\Delta G_{\text{IP}}$  is determined by the interplay of van der Waals and Born energies, which depends on the distance and on the cluster size, as shown in Figure 3. A negative value of  $\Delta G_{\text{IP}}$  means that the attractive forces are prevailing over the repulsive forces, thus decreasing the critical energy barrier to form a stable nucleus.

### 3.2.3. Maximum Relative Decrease in Critical Nucleus Size.

The stabilization effect due to the presence of the seed surface can also be characterized by the maximum of  $\nu(S, x)$ , defined as

$$\lambda^*(S) = \max_x \nu(S, x) \quad (15)$$

When  $\lambda^* \approx 0$ , only homogeneous nucleation occurs, whereas when  $\lambda^* > 0$  and increases toward 1, the stabilization effect is such that nucleation as SNIPE prevails.

### 3.2.4. Compartmentalization of the Stabilization Effect.

From the thermodynamic analysis above, we obtain the Gibbs free energy as a continuous function of  $S$ ,  $n$ , and  $x$  (eq 10), whose formula is accurate and insightful, but its distance dependence makes it difficult to incorporate it in macroscopic descriptions of crystallization.<sup>1</sup>

To simplify the  $x$ -dependence of  $\Delta G$ , we can compartmentalize the space into two regions: the stabilization region ( $0 < x/d_1 \leq l_{\text{st}}$ ) and the bulk region ( $x/d_1 > l_{\text{st}}$ ). In the stabilization region, the formation of a cluster is dependent on the interparticle energies and  $E_{\text{st}} > 1$ , whereas in the bulk region, the stabilization effect is absent and  $E_{\text{st}} = 1$ , whereby only homogeneous nucleation can occur.

The volume of the stabilization compartment is directly proportional to  $l_{\text{st}}$  and to the total area of seed crystals present in the system, i.e., the second moment of the seed crystal population. In Part II of this series,<sup>56</sup> calculations of these compartment volumes are presented.

For simplicity, the two-compartment  $\Delta G$  can be described by a piecewise constant function  $\Delta \bar{G}$  as

$$\Delta \bar{G}(S, n, x) = \begin{cases} -nk_{\text{B}}T \ln(S\tilde{E}_{\text{st}}(n)) + b\gamma n^{2/3} & 0 < x/d_1 \leq l_{\text{st}} \\ -nk_{\text{B}}T \ln S + b\gamma n^{2/3} & x/d_1 > l_{\text{st}} \end{cases} \quad (16)$$

where  $\tilde{E}_{\text{st}}(n) = E_{\text{st}}(n, \tilde{x}_n)$ , with  $\tilde{x}_n$  being the distance corresponding to the minimum of  $\Delta G_{\text{IP}}$  for a specific cluster size  $n$  (see the red dashed line in Figure 6). The choice of the minimum of  $\Delta G_{\text{IP}}$ , thus the maximum of  $E$ , is driven by the fact that the minimum in energy corresponds to the most energetically stable location for a cluster, hence to its preferred location.

In Figure 7, we plot the values of  $\tilde{E}_{\text{st}}(n)$  thus obtained; it is apparent that it is a monotonically decreasing function of  $n$ . In

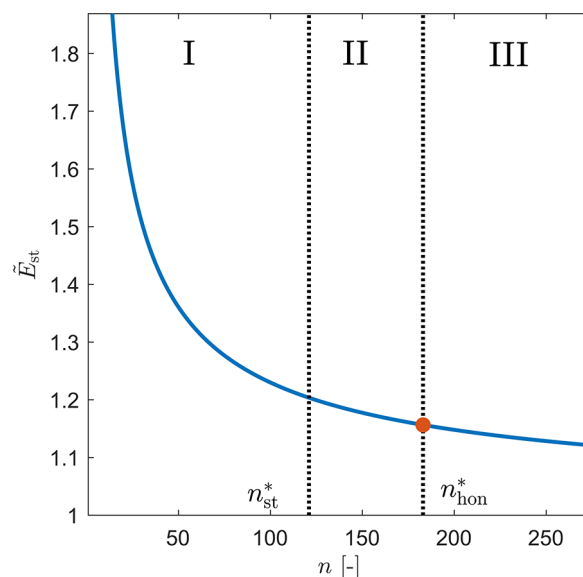


**Figure 7.**  $\tilde{E}_{\text{st}}$  as a function of  $n$ . Region II, where  $n_{\text{st}}^* < n < n_{\text{hon}}^*$ , corresponds to cluster sizes that can undergo secondary nucleation thanks to the interparticle energy effect described by SNIPE. In the current case,  $S = 1.7$  and  $\tilde{E}_{\text{st}}(n_{\text{hon}}^*) = 1.17$  (red dot).

particular, the reader should focus on region II, where  $n_{\text{st}}^* < n < n_{\text{hon}}^*$ , which corresponds to the range of cluster sizes that can undergo nucleation because of the stabilization effect.

It is also worth noting that for some applications, a simplification would be useful, whereby in the compartment where stabilization is active, the enhancement factor is constant. We call such constant enhancement factor  $\bar{E}_{\text{st}}$  and we choose to assign it the value corresponding to the critical nucleus size calculated from CNT, i.e., we set  $\bar{E}_{\text{st}} = \tilde{E}_{\text{st}}(n_{\text{hon}}^*)$ . In the current case,  $\bar{E}_{\text{st}} = \tilde{E}_{\text{st}}(n_{\text{hon}}^*) = 1.17$ . From the inspection of Figure 7, one can readily observe that this is a rather conservative choice that most likely underestimates the intensity of the stabilization effect predicted by the SNIPE theory.

**3.3. Effect of Supersaturation.** The effect of supersaturation on the three key indicators defined above is shown in Figure 8 (see the corresponding energy landscapes in Figures 5a,b and 4 as a reference for the values  $S = 1.5, 1.9$ , and  $1.7$ , respectively). One can observe that by increasing the supersaturation, the stabilization effect is monotonically enhanced, as indicated by the stabilization indicators  $E_{\text{st}}(n_{\text{hon}}^*)$ , and  $\lambda^*$  (whose values are given by the left axis of Figure 8). The stabilization distance (right axis of Figure 8) is less sensitive to supersaturation, but it also monotonically increases, thus indicating that the distance at which the stabilization effect is active increases with supersaturation.

## 4. DISCUSSION AND CONCLUSIONS

**4.1. Sensitivity Analysis.** The parameters used in this study, i.e., those given in Table 1, based on similar studies in the literature,<sup>33,34,36,48</sup> are admittedly difficult to measure. For this reason, we have performed a sensitivity analysis with respect to the Hamaker constant of the cluster,  $A_{\text{c}}$ , and to the collision diameter in the Born repulsive energy contribution,  $\sigma_0$ , and have illustrated it in Figure 9, using as reference value  $S = 1.7$ .



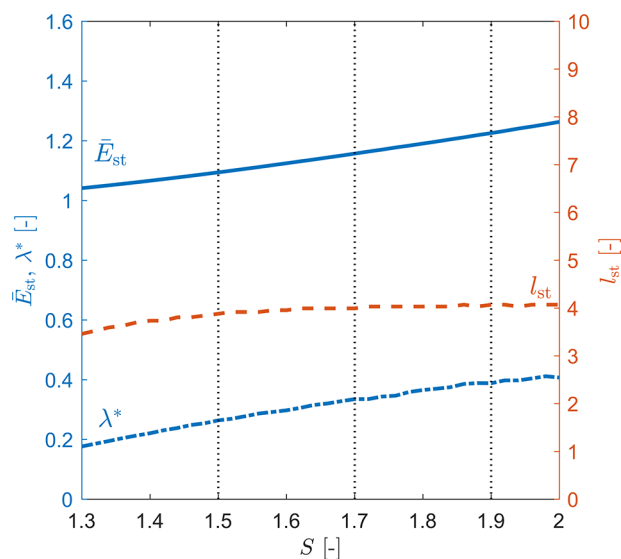


**Figure 8.** Effect of the variation of  $S$  on the supersaturation enhancement factor (solid blue line) (left axis), on the maximum relative decrease in critical nucleus size (dash-dotted black line) (left axis), and on the stabilization distance (dashed red line) (right axis). The dashed vertical lines correspond to  $S = 1.5, 1.7,$  and  $1.9$ , whose energy landscapes are reported in Figures 4 and 5.

The three stabilization indicators are plotted in Figure 9, namely, the supersaturation enhancement factor, i.e.,  $\bar{E}_{st}$  as a solid blue line, and the maximum relative decrease in critical nucleus size, i.e.,  $\lambda^*$ , as a dash-dotted blue line, using the left vertical axis (dimensionless), and the stabilization distance, i.e.,  $l_{st}$  as a dashed red line, using the right vertical axis (in units corresponding to the number of molecular diameters). The plot on the left illustrates the effect of changing the Hamaker constant,  $A_c$ , at constant collision diameter,  $\sigma_0$ , whereas the plot on the right illustrates the effect of changing the latter at constant values of the former.

It can readily be observed that, on the one hand, increasing the Hamaker constant enhances the stabilization effect, as quantified

by all three indicators. This is consistent with the fact that the interparticle energy introduced by the SNIPE model becomes larger and larger relative to the energy associated with the formation of an  $n$ -sized cluster in the CNT with increasing values of the Hamaker constant (see eq 7 with eq 5).

On the other hand, increasing the action range of the Born repulsive forces, i.e., increasing  $\sigma_0$ , weakens the stabilization effect, particularly it decreases the supersaturation enhancement factor and the maximum relative decrease in critical nucleus size. The stabilization distance remains unaffected in this range of values of  $\sigma_0$  because it is mostly affected by the longer-range attractive van der Waals forces.

In summary, a stronger stabilization effect, thus an enhancement of secondary nucleation, can be obtained in systems that exhibit larger Hamaker constants and smaller collision diameters.

#### 4.2. Comparison with ECSN and Change of System.

The established ECSN theory describes the process of “catastrophic” secondary nucleation in the presence of seed crystals and in the absence of attrition. It is acknowledged to be able to explain and to describe the non-stereo-selective secondary nucleation of enantiomers that has been observed in some experimental systems.<sup>8,26,27,57</sup>

**4.2.1. Thermodynamics of ECSN.** The thermodynamic foundations of ECSN and SNIPE are the same in that they both include interparticle energies to describe the formation (and the stabilization) of a cluster close to the seed surface. Nevertheless, ECSN is based on some stricter hypotheses than those required by SNIPE, namely:

- (1) ECSN considers only van der Waals attractive forces but no short-range repulsive ones.
- (2) In the derivation of the Hamaker equation for the interparticle energies (see the first term in eq 5), the expression of the van der Waals energy is simplified for the close approach case ( $x \ll R_n$ ), resulting in

$$E_{IP,ECSN}^c(n, x) = -\frac{A_c R_n}{6x} \quad (17)$$

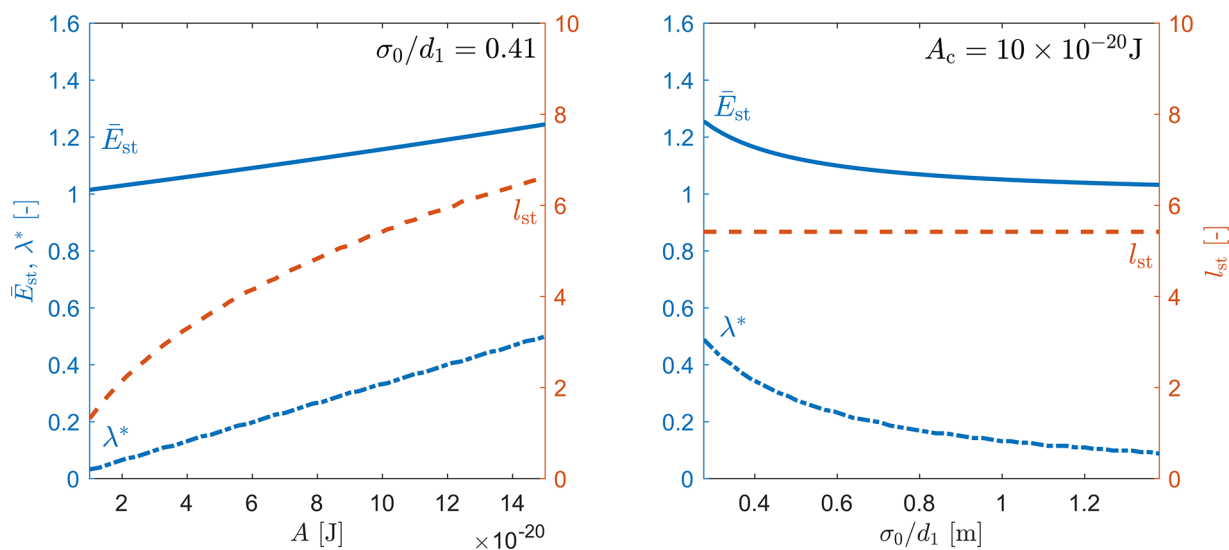


**Figure 9.** Effect of the variation of two uncertain parameters, i.e., Hamaker constant of the cluster,  $A_c$  (left), and the collision diameter in the Born repulsive energy,  $\sigma_0$  (right). The supersaturation enhancement factor is shown with solid blue lines (left axis), the maximum relative decrease in critical nucleus size is shown with dash-dotted blue lines (left axis), and the stabilization distance is shown with dashed red lines (right axis).

- (3) In the calculation of the interparticle potential, no contribution of the solute molecules in solution is taken into account since they are considered indistinguishable from the solvent molecules: this corresponds to setting  $A_m = 0$  in the analysis above (see eq 7).

The complete Gibbs free energy change upon formation of a cluster according to the ECSN is therefore

$$\Delta G_{\text{ECSN}}(S, n, x) = \Delta G_{\text{hon}}(S, n) - E_{\text{IP,ECSN}}^c(n, x) \quad (18)$$

which can be directly compared to eq 4 for SNIPE.

The system analyzed both theoretically and experimentally by Qian and Botsaris<sup>5</sup> is potassium chloride in an aqueous solution. Considering that KCl dissociates in aqueous solution, recent studies<sup>49–51</sup> show that a more comprehensive thermodynamic analysis should include the electrostatic contribution, in addition to van der Waals and Born energies (see also Section 2.1).

Finally, it is worth noting that for nondissociating systems, the thermodynamics derived in SNIPE is more general than that derived in ECSN, and that these two thermodynamic descriptions are applied to two different kinetic frameworks, as described below.

**4.2.2. Kinetics of ECSN and Secondary Nucleation Rate.** From the kinetics perspective, the ECSN model assumes that, in the thin layer where stabilization is active, subcritical molecular clusters of a fixed size grow by aggregation, through the so-called von Smoluchowski rapid coagulation.<sup>58</sup> Through further considerations about the coagulation process, the thickness of the stabilization layer, and the area of the seed crystal, a secondary nucleation rate for ECSN has been derived and applied to discuss experimental data.<sup>5</sup>

**4.3. Concluding Remarks.** In the framework of the classical nucleation theory, we have presented a novel approach to explain secondary nucleation close to the surface of a seed crystal. The analysis takes into consideration the interparticle forces that a cluster experiences in the proximity of a seed crystal, namely, van der Waals attractive forces and Born repulsive forces, and it includes them into the expression of the Gibbs free energy of formation of a cluster. From this, a critical cluster size and an energy barrier for nucleation can be calculated, similarly to what is done in the classical nucleation theory. The novelty of this work lies in an extension of the CNT by including the interparticle forces as an external field for describing a secondary nucleation mechanism that is not due to attrition.

The addition of interparticle forces in the calculation of the Gibbs free energy for nucleation results in the stabilization of subcritical clusters close to the seed surface. At a long distance from the seed surface, the developed model is reduced to homogeneous nucleation according to the classical nucleation theory (CNT). The approach has been analyzed for different supersaturation levels of paracetamol crystallization in an ethanol solution. Moreover, the sensitivity analysis allowed us to highlight the importance of the choice of two parameters, namely, the Hamaker constant and the collision diameter, for the stabilization of the crystallization process.

The intensity of the stabilization effect due to the seed surface can be quantified in terms of some key quantities, one of which is the enhanced supersaturation factor,  $E_{\text{st}}$ . In Part II of this series, this quantity has been implemented in the framework of the kinetic rate equations model to describe the kinetics of secondary nucleation by interparticle energies. We are confident that such an approach can be used also for many systems and

conditions, given the knowledge of the interparticle forces acting in the systems and the key parameters to model them.

Summarizing, the theory above can be useful to provide the basis for the description of secondary nucleation in crystallizers, where attrition and mechanical collisions are not the dominant mechanisms, but secondary nucleation, due to the presence of seed crystals and possibly shear, plays the main role in generating new crystals and determining the final product's quality. An additional potential issue, which is out of the scope of this work, concerns the removal of nuclei from the seed surface to the bulk of the solution. According to the literature,<sup>24,59,60</sup> the removal can be triggered by fluid shear transporting nuclei away from the seed surface. In this case, the supercritical cluster, which is larger compared to molecules and subcritical clusters, would experience inertial forces, e.g., drag and shear, resulting in the removal of such a large supercritical cluster from the seed surface.

In Parts II and III of this series, the following approach is adopted. First, based on the thermodynamics developed here, a kinetic model for SNIPE, which simultaneously describes homogeneous nucleation, growth, and secondary nucleation by interparticle energies while overcoming the limitations of the ECSN model, is developed (Part II). Then, based on the thermodynamic and kinetics models, an expression for the secondary nucleation rate according to SNIPE is derived (Part III). To this aim, Part II extends the conventional kinetic rate equation (KRE) model of nucleation by including a description of SNIPE, while Part III compares different models of secondary nucleation rates (including ECSN) with real and virtual experiments on different materials.

## ■ ASSOCIATED CONTENT

### SI Supporting Information

The Supporting Information is available free of charge at <https://pubs.acs.org/doi/10.1021/acs.cgd.1c00927>.

Analysis of growth mechanisms, concentration profile close to the surface of a growing crystal, and a thorough derivation for the interparticle energies for monomer and clusters (PDF)

## ■ AUTHOR INFORMATION

### Corresponding Authors

Luca Bosetti – Institute of Energy and Process Engineering, ETH Zurich, 8092 Zurich, Switzerland; [orcid.org/0000-0001-6657-6510](https://orcid.org/0000-0001-6657-6510); Email: [bosettl@ipe.mavt.ethz.ch](mailto:bosettl@ipe.mavt.ethz.ch)

Byeongho Ahn – Institute of Energy and Process Engineering, ETH Zurich, 8092 Zurich, Switzerland; [orcid.org/0000-0002-4405-5041](https://orcid.org/0000-0002-4405-5041); Email: [ahn@ipe.mavt.ethz.ch](mailto:ahn@ipe.mavt.ethz.ch)

Marco Mazzotti – Institute of Energy and Process Engineering, ETH Zurich, 8092 Zurich, Switzerland; [orcid.org/0000-0002-4948-6705](https://orcid.org/0000-0002-4948-6705); Email: [marco.mazzotti@ipe.mavt.ethz.ch](mailto:marco.mazzotti@ipe.mavt.ethz.ch)

Complete contact information is available at: <https://pubs.acs.org/10.1021/acs.cgd.1c00927>

### Notes

The authors declare no competing financial interest.

## ■ ACKNOWLEDGMENTS

This project received funding from the European Research Council (ERC) under the European Union's Horizon 2020 Research and Innovation Programme under Grant Agreement No. 788607.

## NOMENCLATURE

### Acronyms

CNT	classical nucleation theory
ECSN	embryo coagulation secondary nucleation
HON	homogeneous nucleation
SNIPE	secondary nucleation caused by interparticle energies

### GREEK SYMBOLS

$\Delta\mu$	driving force for crystallization [J]
$\gamma$	specific surface energy [J m <sup>-2</sup> ]
$\rho$	density [kg m <sup>-3</sup> ]
$\sigma_0$	collision diameter [m]

### ROMAN SYMBOLS

$A$	Hamaker constant [J]
$b$	surface area of a solute molecule [m <sup>2</sup> ]
$c$	solute concentration [kg kg <sup>-1</sup> ]
$c^*$	solubility concentration [kg kg <sup>-1</sup> ]
$d$	diameter [m]
$E_{st}$	strength of the stabilization effect
$k_B$	Boltzmann constant [J K <sup>-1</sup> ]
$k_v$	volume shape factor
$l_{st}$	effective range of the stabilization effect
$M_w$	molecular weight [kg mol <sup>-1</sup> ]
$n$	cluster size in terms of the number of solute molecules
$N_A$	Avogadro number [mol <sup>-1</sup> ]
$R$	radius [m]
$S$	supersaturation
$T$	absolute temperature [K]
$V$	volume [m <sup>3</sup> ]
$x$	surface-to-surface distance [m]
$\Delta G$	Gibbs free energy for forming a molecular cluster [J]

### SUPERSCRIPTS AND SUBSCRIPTS

$n$	$n$ -sized clusters
$B$	Born repulsion
$c$	cluster/crystal
$I$	interface
$IP$	interparticle
$l$	liquid/solution
$m$	molecule
$se$	seed crystals
$vdW$	van der Waals

### REFERENCES

- (1) Kashchiev, D. *Nucleation*; Elsevier Inc., 2000.
- (2) Davey, R.; Garside, J. *From Molecules to Crystallizers*; Oxford University Press, 2000.
- (3) Garside, J.; Jančić, S. J. Measurement and scale-up of secondary nucleation kinetics for the potash alum-water system. *AIChE J.* **1979**, *25*, 948–958.
- (4) Agrawal, S. G.; Paterson, A. H. J. Secondary Nucleation: Mechanisms and Models. *Chem. Eng. Commun.* **2015**, *202*, 698–706.
- (5) Qian, R. Y.; Botsaris, G. D. A new mechanism for nuclei formation in suspension crystallizers: The role of interparticle forces. *Chem. Eng. Sci.* **1997**, *52*, 3429–3440.
- (6) Zhang, D.; Wang, X.; Ulrich, J.; Tang, W.; Xu, S.; Li, Z.; Rohani, S.; Gong, J. Control of Crystal Properties in a Mixed-Suspension Mixed-Product Removal Crystallizer: General Methods and the Effects of Secondary Nucleation. *Cryst. Growth Des.* **2019**, *19*, 3070–3084.
- (7) Mersmann, A. *Crystallization Technology Handbook*, 2nd ed.; Marcel Dekker, Inc., 2001.
- (8) Steendam, R. R.; Frawley, P. J. Secondary Nucleation of Sodium Chlorate: The Role of Initial Breeding. *Cryst. Growth Des.* **2019**, *19*, 3453–3460.
- (9) van der Heijden, A. E. D. M.; van der Eerden, J. P.; van Rosmalen, G. M. The Secondary Nucleation Rate: a physical model. *Chem. Eng. Sci.* **1994**, *49*, 3103–3113.
- (10) Denk, E. G.; Botsaris, G. D. Fundamental studies in secondary nucleation from solution. *J. Cryst. Growth* **1972**, *13–14*, 493–499.
- (11) Clontz, N. A.; McCabe, W. L. In *Contact Nucleation of Magnesium Sulfate Heptahydrate*, Chemical Engineering Symposium Series No. 110, 1971; pp 6–17.
- (12) Cui, Y.; Stojakovic, J.; Kijima, H.; Myerson, A. S. Mechanism of Contact-Induced Heterogeneous Nucleation. *Cryst. Growth Des.* **2016**, *16*, 6131–6138.
- (13) Anwar, J.; Khan, S.; Lindfors, L. Secondary crystal nucleation: Nuclei breeding factory uncovered. *Angew. Chem., Int. Ed.* **2015**, *54*, 14681–14684.
- (14) Xu, S.; Wang, Y.; Hou, Z.; Chuai, X. Overview of secondary nucleation: From fundamentals to application. *Ind. Eng. Chem. Res.* **2020**, *59*, 18335–18356.
- (15) Yousuf, M.; Frawley, P. J. Quantitative Link between Secondary Nucleation and Mixing Hydrodynamics in Batch Cooling Crystallization: A New Approach in Process Development. *Org. Process Res. Dev.* **2019**, *23*, 2009–2019.
- (16) Gahn, C.; Mersmann, A. Theoretical Prediction and Experimental Determination of Attrition Rates. *Chem. Eng. Res. Des.* **1997**, *75*, 125–131.
- (17) Gahn, C.; Mersmann, A. Brittle fracture in crystallization processes Part A. Attrition and abrasion of brittle solids. *Chem. Eng. Sci.* **1999**, *54*, 1273–1282.
- (18) Bermingham, S. K. A Design Procedure and Predictive Models for Solution Crystallisation Processes. Ph.D. Thesis, T.U. Delft, 2003.
- (19) Bosetti, L.; Mazzotti, M. Study of Secondary Nucleation by Attrition of Potassium Alum Crystals Suspended in Different Solvents. *Cryst. Growth Des.* **2020**, *20*, 2570–2577.
- (20) Larson, M. A.; Garside, J. Solute clustering in supersaturated solutions. *Chem. Eng. Sci.* **1986**, *41*, 1285–1289.
- (21) Mullin, J. W.; Leci, C. L. Evidence of molecular cluster formation in supersaturated solutions of citric acid. *Philos. Mag.* **1969**, *19*, 1075–1077.
- (22) Cui, Y.; Myerson, A. S. Experimental evaluation of contact secondary nucleation mechanisms. *Cryst. Growth Des.* **2014**, *14*, 5152–5157.
- (23) Wong, S. Y.; Cui, Y.; Myerson, A. S. Contact secondary nucleation as a means of creating seeds for continuous tubular crystallizers. *Cryst. Growth Des.* **2013**, *13*, 2514–2521.
- (24) Yousuf, M.; Frawley, P. J. Experimental Evaluation of Fluid Shear Stress Impact on Secondary Nucleation in a Solution Crystallization of Paracetamol. *Cryst. Growth Des.* **2018**, *18*, 6843–6852.
- (25) Sung, C. Y.; Estrin, J.; Youngquist, G. R. Secondary Nucleation of Magnesium Sulfate by Fluid Shear. *AIChE J.* **1973**, *19*, 957–962.
- (26) Buhse, T.; Durand, D.; Kondepudi, D.; Laudadio, J.; Spilker, S. Chiral symmetry breaking in crystallization: the role of convection. *Phys. Rev. Lett.* **2000**, *84*, 4405–4408.
- (27) Cameli, F.; ter Horst, J. H.; Steendam, R. R.; Xiouras, C.; Stefanidis, G. D. On the Effect of Secondary Nucleation on Deracemization through Temperature Cycles. *Chem. – Eur. J.* **2020**, *26*, 1344–1354.
- (28) Kashchiev, D.; Vekilov, P. G.; Kolomeisky, A. B. Kinetics of two-step nucleation of crystals. *J. Chem. Phys.* **2005**, *122*, No. 244706.
- (29) Vekilov, P. G.; Vorontsova, M. A. Nucleation precursors in protein crystallization. *Acta Crystallogr., Sect. F* **2014**, *70*, 271–282.
- (30) Salvalaglio, M.; Mazzotti, M.; Parrinello, M. Urea homogeneous nucleation mechanism is solvent dependent. *Faraday Discuss.* **2015**, *179*, 291–307.
- (31) Gebauer, D.; Kellermeier, M.; Gale, J. D.; Bergström, L.; Cölfen, H. Pre-nucleation clusters as solute precursors in crystallisation. *Chem. Soc. Rev.* **2014**, *43*, 2348–2371.

- (32) Verwey, E. J.; Overbeek, J. T. G. *Theory of the Stability of Lyophobic Colloids*; Elsevier Inc., 1955.
- (33) Ruckenstein, E.; Prieve, D. C. Adsorption and desorption of particles and their chromatographic separation. *AIChE J.* **1976**, *22*, 276–283.
- (34) Feke, D. L.; Prabhu, N. D.; Mann, J. A.; Mann, J. A. A formulation of the short-range repulsion between spherical colloidal particles. *J. Phys. Chem. A.* **1984**, *88*, 5735–5739.
- (35) Derjaguin, B.; Landau, L. Theory of the stability of strongly charged lyophobic sols and of the adhesion of strongly charged particles in solutions of electrolytes. *Prog. Surf. Sci.* **1993**, *43*, 30–59.
- (36) Ren, Z.; Harshe, Y. M.; Lattuada, M. Influence of the potential well on the breakage rate of colloidal aggregates in simple shear and uniaxial extensional flows. *Langmuir* **2015**, *31*, 5712–5721.
- (37) Harshe, Y. M.; Lattuada, M. Breakage rate of colloidal aggregates in shear flow through Stokesian dynamics. *Langmuir* **2012**, *28*, 283–292.
- (38) Söhnel, O.; Garside, J. Solute clustering and nucleation. *J. Cryst. Growth* **1988**, *89*, 202–208.
- (39) Mullin, J. W. *Industrial Crystallization*; Springer, 1976.
- (40) Tai, C. Y.; McCabe, W. L.; Rousseau, R. W. Contact nucleation of various crystal types. *AIChE J.* **1975**, *21*, 351–358.
- (41) Myerson, A. S. et al. *Handbook of Industrial Crystallization*; Elsevier Inc., 2015; pp 20–23.
- (42) Pan, W.; Vekilov, P. G.; Lubchenko, V. Origin of anomalous mesoscopic phases in protein solutions. *J. Phys. Chem. B* **2010**, *114*, 7620–7630.
- (43) Tai, C. Y.; Wu, J. F.; Rousseau, R. W. Interfacial supersaturation, secondary nucleation, and crystal growth. *J. Cryst. Growth* **1992**, *116*, 294–306.
- (44) Rosenberger, F. Inorganic and protein crystal growth - similarities and differences. *J. Cryst. Growth* **1986**, *76*, 618–636.
- (45) Eder, C.; Choszcz, C.; Müller, V.; Briesen, H. Jamin-interferometer-setup for the determination of concentration and temperature dependent face-specific crystal growth rates from a single experiment. *J. Cryst. Growth* **2015**, *426*, 255–264.
- (46) Miyashita, S.; Komatsu, H.; Suzuki, Y.; Nakada, T. Observation of the concentration distribution around a growing lysozyme crystal. *J. Cryst. Growth* **1994**, *141*, 419–424.
- (47) Hamaker, H. C. The London-van der Waals attraction between spherical particles. *Physica* **1937**, *4*, 1058–1072.
- (48) Israelachvili, J. N. Nonequilibrium and Time-Dependent Interactions. In *Intermolecular and Surface Forces*; Elsevier, 2011; pp 169–188.
- (49) Finney, A. R.; McPherson, I. J.; Unwin, P. R.; Salvalaglio, M. Electrochemistry, ion adsorption and dynamics in the double layer: a study of NaCl(aq) on graphite. *Chem. Sci.* **2021**, *12*, 11166–11180.
- (50) Jiang, H.; Debenedetti, P. G.; Panagiotopoulos, A. Z. Nucleation in aqueous NaCl solutions shifts from 1-step to 2-step mechanism on crossing the spinodal. *J. Chem. Phys.* **2019**, *150*, No. 124502.
- (51) Zimmermann, N. E.; Vorselaars, B.; Quigley, D.; Peters, B. Nucleation of NaCl from Aqueous Solution: Critical Sizes, Ion-Attachment Kinetics, and Rates. *J. Am. Chem. Soc.* **2015**, *137*, 13352–13361.
- (52) Joung, I. S.; Cheatham, T. E. Determination of alkali and halide monovalent ion parameters for use in explicitly solvated biomolecular simulations. *J. Phys. Chem. B* **2008**, *112*, 9020–9041.
- (53) Worlitschek, J.; Mazzotti, M. Model-based optimization of particle size distribution in batch-cooling crystallization of paracetamol. *Cryst. Growth Des.* **2004**, *4*, 891–903.
- (54) Li, H.; Kawajiri, Y.; Grover, M. A.; Rousseau, R. W. Modeling of nucleation and growth kinetics for unseeded batch cooling crystallization. *Ind. Eng. Chem. Res.* **2017**, *56*, 4060–4073.
- (55) Kashchiev, D.; van Rosmalen, G. M. Review: Nucleation in solutions revisited. *Cryst. Res. Technol.* **2003**, *38*, 555–574.
- (56) Ahn, B.; Bosetti, L.; Mazzotti, M. Secondary Nucleation by Interparticle Energies. II. Kinetics. *Cryst. Growth Des.*, 2021 DOI: 10.1021/acs.cgd.1c00928
- (57) Prasanna, P. R. M.; Botsaris, G. D. In *Modeling Polymorphic Embryos and Their Relevance to Preferential Crystallization: Extending EC3N to Polymorphic Systems*, AIChE Annual Meeting, 1982.
- (58) von Smoluchowski, M. Versuch einer mathematischen Theorie der Koagulationskinetik kolloider Loesungen. *Ann. Phys.* **1917**, *270*, 222–240.
- (59) Liu, J.; Rasmuson, A. C. Influence of agitation and fluid shear on primary nucleation in solution. *Cryst. Growth Des.* **2013**, *13*, 4385–4394.
- (60) Forsyth, C.; Burns, I. S.; Mulheran, P. A.; Sefcik, J. Scaling of Glycine Nucleation Kinetics with Shear Rate and Glass-Liquid Interfacial Area. *Cryst. Growth Des.* **2016**, *16*, 136–144.

**HAZARD AWARENESS  
REDUCES LAB INCIDENTS**

**ACS Essentials of  
Lab Safety for  
General Chemistry**

A new course from the  
American Chemical Society

ACS Institute  
Learn. Develop. Excel.

EXPLORE  
ORGANIZATIONAL  
SALES  
solutions.acs.org/essentialsolabsafety

REGISTER FOR  
INDIVIDUAL ACCESS  
institute.acs.org/courses/essentials-lab-safety.html